IRJSE International Research Journal of Science & Engineering
Int. Res. J. of Science & Engineering, Volume 14 (2) 2026
ISSN: 2322-0015
SJIF Impact Factor 6.137
https://doi.org/10.5281/zenodo.19712708
RESEARCH ARTICLE OPEN ACCESS

Camphor Sulfonic Acid-Assisted Synthesis of PANI/V_2O_5 Composite: Structural, Spectroscopic and Electrochemical Investigations

Vikrant P. Lalge[1] Harshad N. Vekhande[1], Tanaji P. Gujar[2] and Jayashree A. Bagawade[1*]

[1]PG Department & research centre of Physics, Vidya Pratishthan's Arts, Science and Commerce College, Baramati, India 413133.
[2]Department of Physics, ADT's Shardabai Pawar Arts, Commerce and Science College, Shardanagar, Baramati, (MS), India 413115.
*Correspondence: Jayashree A. Bagawade (chimanpurejayu@gmail.com)

Manuscript Details

Received :11.04.2026
Accepted: 27.04.2026
Published: 3030.04.2026

Available online on https://www.irjse.in
ISSN: 2322-0015

Cite this article as:
Vikrant P. Lalge, Harshad N. Vekhande, Tanaji P. Gujar and Jayashree A. Bagawade. Camphor Sulfonic Acid-Assisted Synthesis of PANI/V_2O_5 Composite: Structural, Spectroscopic and Electrochemical Investigations, *Int. Res. Journal of Science & Engineering*, 2026, Volume 14(2): 101-111.
https://doi.org/10.5281/zenodo.19712708

Abstract

The present study details the synthesis and characterization of camphor sulfonic acid (CSA) ($C_{10}H_{16}O_4S$)-synthesized polyaniline (PANI-CSA) and its PANI-CSA/V_2O_5 composite, which incorporates 50 wt. % Vanadium Pentoxide (V_2O_5). The composite was synthesized via the in situ oxidative polymerization of aniline ($C_6H_5NH_2$), employing CSA as the dopant and Ammonium Persulfate (APS) [$(NH_4)_2S_2O_8$] as the oxidizing agent, with V_2O_5 functioning as both the vanadium source and structural dopant. Characterization of the synthesized PANI-CSA and PANI-CSA/V_2O_5 composites was conducted using UV-visible spectroscopy, X-ray diffraction (XRD), Fourier-transform infrared spectroscopy (FTIR), field-emission scanning electron microscopy (FE-SEM), high-resolution transmission electron microscopy (HR-TEM), and Raman spectroscopy. XRD analysis indicated that PANI-CSA was predominantly amorphous, whereas the composite displayed distinct crystalline peaks of V_2O_5. FTIR and Raman spectroscopy confirmed robust chemical interactions between PANI-CSA and V_2O_5. Observations from FE-SEM and HR-TEM revealed significant morphological changes and the emergence of a distinct layered crystalline structure within the composites. Cyclic Voltammetry (CV) demonstrated an enhanced redox current response in PANI-CSA/V_2O_5 compared to pristine PANI-CSA, indicating improved charge transport and electrochemical performance. The amorphous nature of PANI-CSA suggests a lack of long-range order within its matrix, with broad diffraction peaks indicative of short-range correlations typical of disordered polymeric systems. These structural characteristics influence the material's electrical and mechanical properties, thereby affecting its performance in practical applications. The findings underscore the composite's potential for use in energy storage and sensing systems and confirm its successful formation.

Keywords: polyaniline camphor sulfonic acid (PANI-CSA), in-situ polymerization, PANI-CSA/V_2O_5 composite, weak acid synthesis, CIF, characterization.

1. Introduction

Conducting polymers have attracted considerable research interest in recent decades due to their unique combination of electrical conductivity, environmental stability, and ease of synthesis. These materials bridge the gap between conventional insulating polymers and inorganic semiconductors, offering tunable electrical and optical properties along with mechanical flexibility. Owing to these characteristics, conducting polymers have found potential applications in diverse fields such as energy storage devices, electrochromic systems, corrosion protection, catalysis, and chemical and gas sensors [1–3]. Among the various conducting polymers investigated, polyaniline (PANI) has emerged as one of the most extensively studied materials because of its relatively simple synthesis process, low cost of monomer, good environmental stability, and unique reversible redox behavior [4,5]. PANI also exhibits multiple oxidation states such as leucoemeraldine, emeraldine, and pernigraniline, which enable significant modulation of its electrical and optical properties. The electrical conductivity and morphology of PANI can be effectively tailored through different synthesis parameters, including the choice of oxidizing agent, type and concentration of dopant acid, polymerization conditions, and incorporation of inorganic fillers or metal oxides [6]. In particular, acid doping plays a crucial role in converting the insulating emeraldine base form of PANI into the highly conductive emeraldine salt form. Strong protonic acids such as hydrochloric acid and sulfuric acid are commonly used during synthesis to achieve high conductivity. However, PANI synthesized in strongly acidic environments often exhibits certain limitations such as low mechanical strength, partial amorphous nature, structural defects, and relatively poor thermal stability, which can hinder its long-term performance in practical device applications [7]. These drawbacks necessitate the development of strategies to enhance the structural and functional properties of PANI. One promising approach to overcome these limitations is the formation of polymer–inorganic composites, where metal oxides are incorporated into the polymer matrix. The integration of metal oxides with conducting polymers can significantly improve the thermal stability, crystallinity, mechanical strength, and electrochemical activity of the material. Metal oxides such as TiO_2, ZnO, Fe_2O_3, and V_2O_5 have been widely explored for this purpose because they provide additional active interfaces, facilitate charge transfer processes, and improve electron transport pathways within the polymer matrix [8-10]. These hybrid materials often exhibit synergistic properties that are superior to those of the individual components. Among the various metal oxides investigated, vanadium pentoxide (V_2O_5) has attracted significant attention due to its layered crystal structure, multiple oxidation states (V^{5+}/V^{4+}), and strong redox and catalytic properties [11,12]. The incorporation of V_2O_5 into the PANI matrix can enhance electron–ion exchange processes, increase structural ordering, and provide improved charge transport pathways. In addition, the presence of V_2O_5 can contribute to improved crystallinity, enhanced mechanical reinforcement, and increased electrochemical activity, making PANI/ V_2O_5 composites highly promising for applications in gas sensing, energy storage devices such as supercapacitors, and electrochromic systems [13-15]. Another important factor influencing the properties of PANI is the nature of the dopant acid used during synthesis. In contrast to conventional strong acids, weak organic acids such as camphor sulfonic acid (CSA) have been reported to produce PANI with improved morphological uniformity and enhanced environmental stability. CSA possesses a relatively bulky molecular structure, which can effectively intercalate between polymer chains and influence the polymerization kinetics. As a result, CSA-doped PANI often exhibits better chain ordering, improved solubility in organic solvents, and enhanced electrical and mechanical properties compared to PANI doped with small inorganic acids [16,17]. Despite the extensive research on PANI synthesized using strong acids and its composites with metal oxides, studies involving CSA-doped PANI combined with V_2O_5 remain relatively limited. The synergistic interaction between PANI-CSA and V_2O_5 is expected to provide improved structural ordering, enhanced charge transport properties, and better surface morphology, which could be beneficial for advanced functional applications. Therefore, the present

work focuses on the synthesis and comprehensive characterization of PANI-CSA and its composite PANI-CSA/V_2O_5 containing 50 wt.% V_2O_5. The primary objective of this study is to investigate the influence of V_2O_5 incorporation on the structural, optical, and morphological properties of PANI-CSA. Particular emphasis is placed on understanding how the presence of V_2O_5 affects the crystallinity, molecular interactions, and surface morphology of the polymer matrix. The results obtained from this study are expected to provide deeper insight into the structure–property relationship of PANI-CSA/V_2O_5 composites and their potential suitability for advanced functional applications.

2. Materials and method

PANI-CSA was produced through the direct chemical oxidation of aniline using ammonium persulfate (APS) as the oxidizing agent following a well-established and cost-effective chemical method [18,19]. This method was modified with respect to reagent proportions, reaction temperature, and reaction times. Aniline monomer (C_8H_5 NH_2, AR grade). Camphor sulfonic acid (CSA, $C_{10}H_{16}O_4S$), Ammonium Persulfate (APS, $(NH_4)_2S_2O_8$), and Vanadium Pentoxide (V_2O_5) were obtained from Sigma-Aldrich and were used without further refinement. Double-distilled water (DDW) was used as served as the solvent for the polymerization reactions.

2.1 Synthesis of PANI-CSA

In the synthesis depicted in Figure 1, CSA (6.5 g) was dissolved in 400 mL of DDW with continuous stirring. Subsequently, 3 mL of freshly distilled aniline was added dropwise to this solution, with stirring maintained for 30 minutes while keeping the reaction temperature between 0 and 3°C. In a separate beaker, APS (8.5 g) was dissolved in 30 mL of DDW and then added dropwise to the aniline-CSA solution, with continuous stirring within the same temperature range (0-3°C). The solution's color gradually transitioned from colorless to green following the addition of APS, indicating the commencement of the oxidative polymerization of aniline. Upon completion of the reaction, the PANI-CSA precipitate was isolated by filtration and repeatedly washed with DDW to remove oxidant residues, unreacted monomers, and impurities. The resultant product was dried in a hot air oven at 70°C for 7 hours. Finally, the dried material was gently ground to obtain a fine PANI-CSA powder, which was stored in a desiccator for subsequent analysis.

1.2 Synthesis of PANI-CSA/V_2O_5

The PANI-CSA/V_2O_5 composite was synthesized via an in situ oxidative polymerization technique. Initially, a solution comprising 6.5 g of CSA in 400 mL of DDW was prepared, to which 3 mL of aniline was added dropwise under continuous stirring and subjected to ultrasonication for 20 minutes. Subsequently, V_2O_5

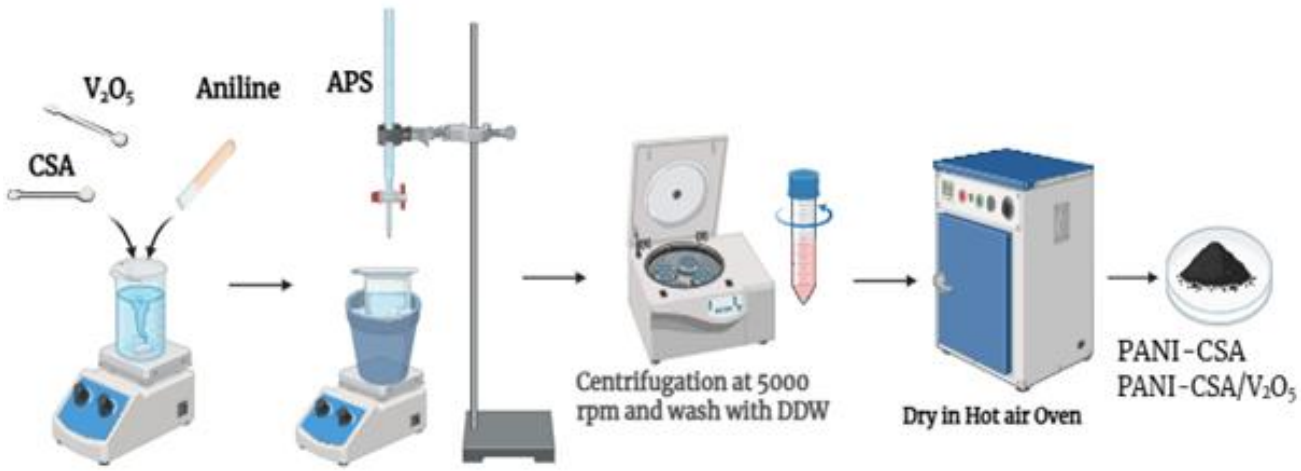

Figure 1 Reaction of PANI-CSA and PANI-CSA/V_2O_5.

powder, constituting 50 wt. % relative to aniline, was dispersed into the solution with persistent stirring. In a separate process, 6.5 g of APS dissolved in 30 mL of DDW was introduced dropwise while maintaining the temperature between 0-3°C using an ice bath. The resultant dark-green precipitate was isolated by centrifugation at 2000 rpm, thoroughly rinsed with DDW, and dried at 70°C for 6 hours. The obtained PANI-CSA/V_2O_5 powder was finely ground and stored in a desiccator until further characterization was conducted. A schematic representation of the PANI-CSA/V_2O_5 composite synthesis is provided.

3. Results and discussions

UV-visible absorption spectra were obtained using a Shimadzu UV–visible spectrophotometer, covering a wavelength range of 200-700 nm. Figure 2 (a, b, c, and d) illustrates the UV-visible spectra of PANI-CSA and the PANI-CSA/V_2O_5 composite, as well as Tauc's relation for both materials, respectively. In Figure 2 (a), two prominent absorption bands for PANI-CSA are observed at 250 nm, along with a low-intensity peak at 330 nm, which are attributed to the π–π* transition of the benzenoid ring, indicating electron excitation within the aromatic structure [20]. The peak at 584 nm is associated with transitions of the quinine-imine group, a characteristic feature in PANI [21]. The PANI-CSA/ V_2O_5 composite displays sharper and more intense absorption peaks at 260 and 330 nm, which are slightly shifted to lower positive values, as depicted in Figure 2 (b). This alteration in the PANI-CSA and PANI-CSA/V_2O_5 composite can be attributed to the polaron concentration [22]. A distinct spectral red shift and an increase in absorption intensity corroborate the strong coupling between the PANI-CSA chains and the V_2O_5 particles [23]. These structural modifications align with the UV-visible spectroscopy results, confirming enhanced electronic delocalization and interaction between the PANI-CSA chains and V_2O_5 particles. The optical bandgap was determined using the indirect Tauc relation.

$$(\alpha h\nu)^{1/2} = A(h\nu - E_g) \quad (1)$$

Where $(\alpha h\nu)^{1/2}$ is plotted of versus photon energy $(\alpha\nu)$, A is constant depending on the transition probability and E_g is band gap energy [24]. The extrapolation of the linear region to the energy axis gave band gap values of 5.5 eV for PANI-CSA by indirect Tauc's relation, as shown in Figure 2 (c), and 5.2 eV for PANI-CSA/V_2O_5, as shown in Figure 2 (d). The decrease in the bandgap after V_2O_5 incorporation indicates the formation of additional localized energy states. This bandgap narrowing suggests enhanced electronic interactions and improved charge transport in the composite material [25].

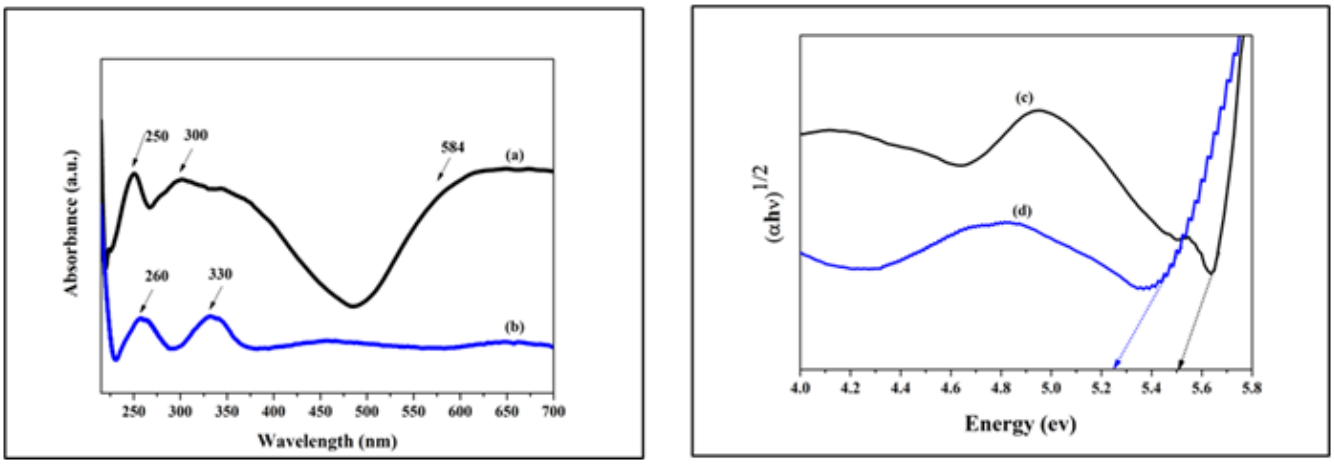

Figure 2 UV-Visible and Tauc's relation, (a) UV-Visible of PANI-CSA, (b) UV-Visible of PANI-CSA/V_2O_5 composite, (c) indirect Tauc's relation of PANI-CSA and (d) indirect Tauc's relation of PANI-CSA/V_2O_5 composite.

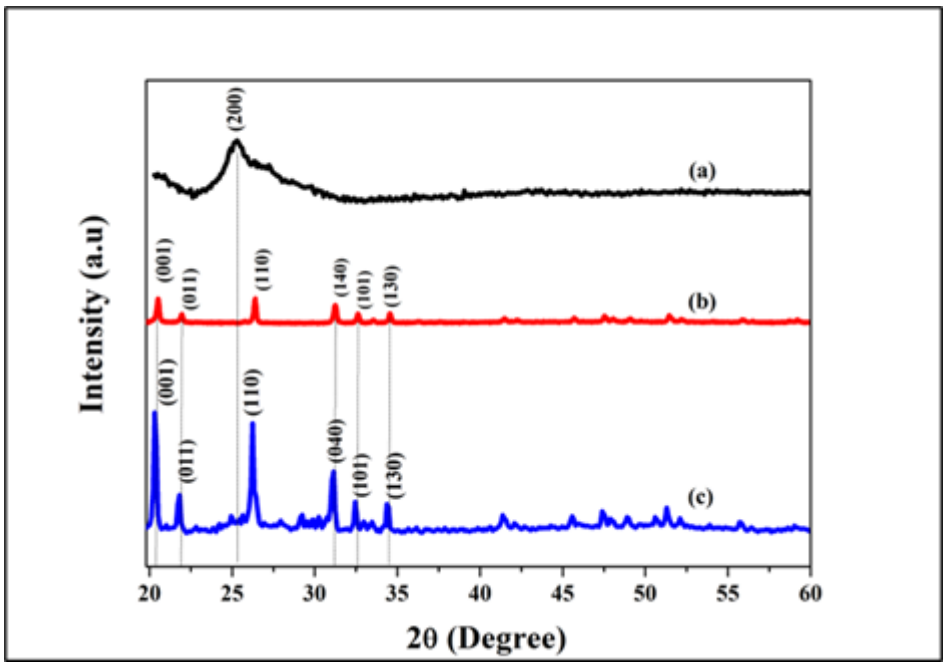

Figure 3 XRD pattern of (a) PANI-CSA, (b) V_2O_5 and (c) PANI-CSA/V_2O_5 composite.

X-ray diffraction analysis was conducted using a Rigaku Miniflex-600 diffractometer with Cu Kα radiation (λ = 0.15425 nm), employing a step size of 0.10^0 and a scan speed of 10^0 min^{-1} over a 2ɵ range of 20^0-60^0. Figure 3 (a, b, and c) show the X-ray Diffraction (XRD) patterns of the PANI-CSA, V_2O_5 and PANI-CSA/V_2O_5 composites, respectively. The broad hump around 2ɵ ≈ 25^0, commonly observed in PANI, indicates the amorphous nature of PANI-CSA (Figure 3a). Furthermore, the well-defined orthorhombic crystalline peaks of V_2O_5 (Figure 3b) suggest the formation of a partially crystalline structure in the PANI-CSA/V_2O_5 composite (Figure 3c). The characteristic peaks at (001) ≈ 20^0, (011) ≈ 21^0, (110) ≈ 26^0, (040) ≈ 31^0, (101) ≈ 32^0, and (130) ≈ 34^0 are present in both the V_2O_5 and PANI-CSA/V_2O_5 composite, consistent with the data (JCPDS No. 98-008-0600). The average crystallite size of V_2O_5 and PANI-CSA/V_2O_5, calculated using the Debye-Scherrer formula, is approximately 38 nm for V_2O_5, while that of the PANI-CSA/V_2O_5 composite is approximately 42 nm. The incorporation of V_2O_5 resulted in a marginal increase in the crystallinity of PANI-CSA, and a comparable enhancement in crystallinity upon V_2O_5 addition has been reported due to the strongly acidic nature of PANI [26]. This suggests that PANI-CSA exhibits relatively improved structural ordering compared to strongly acid-synthesized PANI and is suitable for electrochemical applications.

Fourier Transform Infrared (FTIR) spectroscopy was performed using a Shimadzu IRAffinity-1S spectrometer in the range of 4000-400 cm^{-1} to identify the functional groups and chemical interactions in the synthesized samples. Figure 4 (a, b, and c) present the FTIR spectra of the PANI-CSA, V_2O_5, and PANI-CSA/V_2O_5 composites, respectively. The FTIR spectrum of PANI-CSA (Figure 4a), where prominent absorption bands appear around 781 cm^{-1} for C-H bending vibration and 576 cm^{-1} for C-S stretching vibration from sulphonic acid group, peaks around 1568 cm^{-1} and 1465 cm^{-1} corresponding to C=C, C=N stretching vibrations of the quinoid diamine units (N=Q=N), C-C aromatic ring stretching of the benzenoid diamine unit (N-B-N), broad bands at 1284 cm^{-1} due to C-N stretching vibrations of secondary amine groups, bands around 1141 cm^{-1} corresponds to S=O due to effect of CSA [27]. The peaks at 1697 cm^{-1} and 2937 cm^{-1} correspond to C=O strongly oxidized species and possible contributions from C=C, respectively [28]. The FTIR spectrum of V_2O_5 (Figure 4b) shows characteristic peaks at 1220 cm^{-1}, 1552

cm^{-1}, 1739 cm^{-1} and 2350 cm^{-1} for V=O stretching vibration and H-O-H bending respectively, and the peaks at 3738 cm^{-1} and 3854 cm^{-1} correspond to -OH stretching vibrations [29]. Upon the incorporation of vanadium into PANI-CSA, several characteristic peaks between 1700 cm^{-1} and 500 cm^{-1} of PANI-CSA/V_2O_5 (Figure 4c) became broader, more intense, and exhibited a noticeable shift toward higher wavenumbers, indicating a strong interaction between PANI-CSA and V_2O_5 and possible changes in the electronic environment of the polymer [30]. The spectrum of the PANI-CSA/V_2O_5 composite exhibited noticeable changes compared to that of PANI-CSA. The slight blue shift (toward higher wavenumbers) observed in several peaks between 1700-3860 cm^{-1} can be attributed to weak van der Waals interactions and changes in the local electronic environment, which is commonly observed in PANI [30]. These spectral modifications clearly demonstrate chemical interactions and strong interfacial bonding between the polymer chains and V_2O_5.

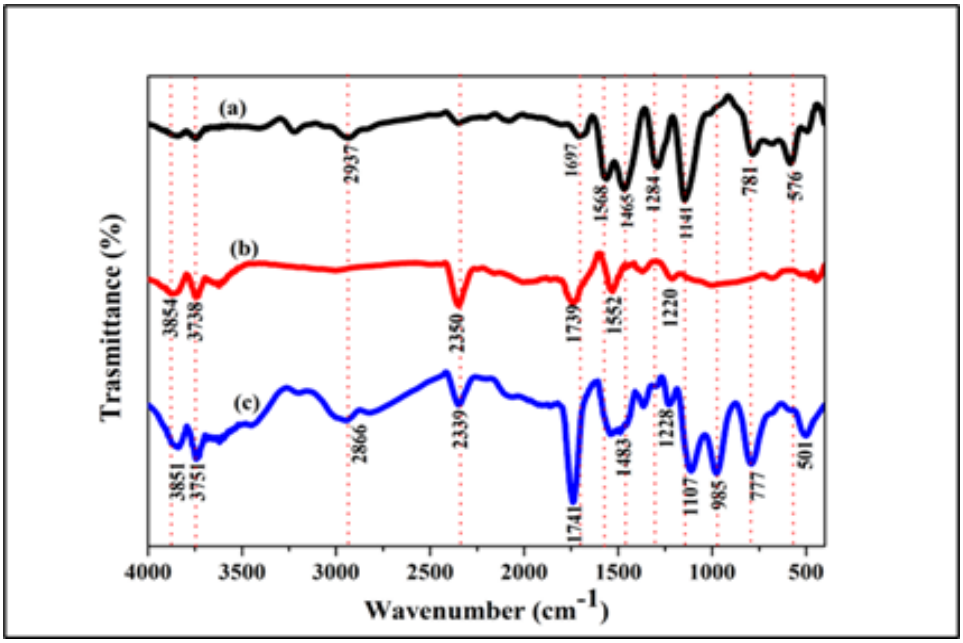

Figure 4 FTIR pattern of (a) PANI-CSA, (b) V_2O_5 and (c) PANI-CSA/V_2O_5 composite

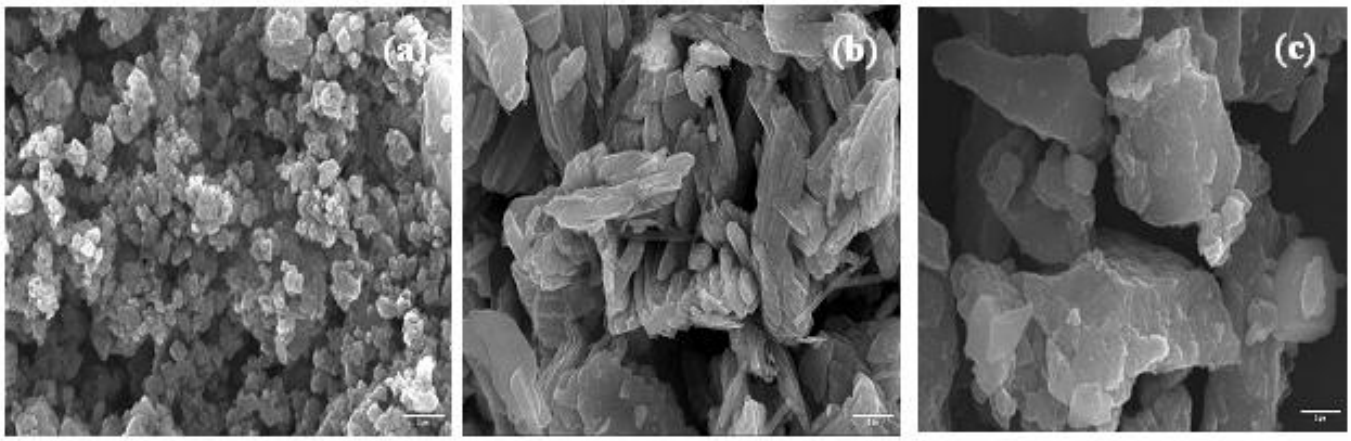

Figure 5 SEM Images of (a) PANI-CSA, (b) V_2O_5 and (c) PANI-CSA/V_2O_5 composite.

The surface morphologies of the PANI-CSA, V_2O_5, and PANI-CSA/V_2O_5 composites were examined using a JEOL JSM-6360F field-emission scanning electron microscope (FE-SEM). Figure 5 (a, b, and c) present FE-SEM micrographs of the PANI-CSA, V_2O_5 and PANI-CSA/V_2O_5 composites, respectively. PANI-CSA (Figure 5a) exhibited a uniformly distributed granular morphology with spherical clusters and an average grain size of 200 nm, which is characteristic of the emeraldine salt form of PANI-CSA [31]. The microstructure of V_2O_5 (Figure 5b) a well-defined crystalline flake-like morphology, indicating its layered oxide nature [32]. In contrast, the PANI-CSA/V_2O_5 composite (Figure 5c) exhibited a distinct morphological transformation. The polymer matrix became denser and more compact with an increase in grain size of approximately 500 nm, with V_2O_5 particles uniformly embedded within the PANI-CSA network. The formation of aggregated clusters suggested strong interfacial interactions within the composite structure. The SEM results are in good agreement with the XRD analysis, wherein the average crystallite size of the PANI-CSA/V_2O_5 composite was calculated to be 42 nm from the XRD measurements, while the grain size estimated from the SEM micrographs was found to be approximately 500 nm, indicating that each grain is composed of multiple crystallites. These morphological changes were consistent with the XRD analyses, confirming the enhanced crystallinity and interfacial interactions in the PANI-CSA/V_2O_5 composite.

The high-resolution morphology of the PANI-CSA, V_2O_5, and PANI-CSA/V_2O_5 composites was observed using a JEOL JEM-2100 Plus High-Resolution Transmission Electron Microscope (HR-TEM). Figure 6 (a, b, and c) show TEM micrographs of the PANI-CSA, V_2O_5, and PANI/V_2O_5 composites, respectively. The TEM image of PANI-CSA (Figure 6a) shows a granular and fibrous morphology with irregularly shaped clusters interconnected throughout the matrix; low-density and semi-transparent regions suggest partial nanostructure exfoliation of porous characteristics typical of amorphous PANI-CSA with a grain size of 200–300 nm, which is commonly observed in strong-acid-synthesized PANI [33]. V_2O_5 (Figure 6b) has a well-defined crystalline morphology consisting of nanorods with smooth sidewalls. The particles appeared to be less agglomerated, confirming their distinct crystalline nature and good dispersion [34]. The V_2O_5 nanorods were uniformly embedded within the PANI-CSA matrix, forming dense and well-integrated nanostructures. The average grain size of the composite ranged from 400 to 500 nm, which is larger than that of the PANI-CSA grain size, indicating strong interfacial coupling and partial crystallinity enhancement due to composite formation.

The observed homogeneous dispersion confirms the effective interaction and excellent interfacial adhesion between the PANI-CSA chains and the V_2O_5 particles. These findings are in good agreement with the XRD and SEM results, collectively confirming that V_2O_5 incorporation leads to improved crystallinity and enhanced structural ordering of PANI-CSA compared to strong acid-synthesized PANI.

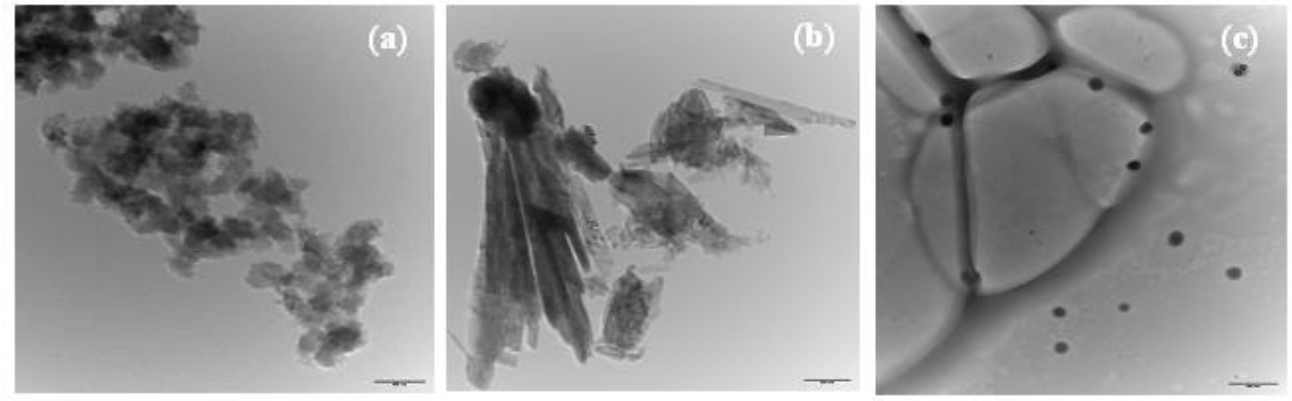

Figure 6 HR-TEM of (a) PANI-CSA, (b) V_2O_5 and (c) PANI-CSA/ V_2O_5 composite.

Raman spectroscopy was carried out using a Renishaw INVIA 0120-20 Raman spectrometer (Renishaw UK) over the wavenumber range of 100-3000 cm^{-1} to investigate the molecular structure and bonding characteristics. Figure 7 (a, b, and c) show the Raman spectra of the PANI-CSA, V_2O_5, and PANI-CSA/ V_2O_5 composites, respectively. The Raman spectrum of PANI-CSA (Figure 7a) exhibits characteristic shoulder at 1174 cm^{-1} corresponding to C-H bending vibrations of the benzenoid ring and a prominent peak at 1595 cm^{-1} represents the C=C stretching vibration of the quinoid ring and peak at 1331 cm^{-1} corresponding to C-N^+ stretching vibration confirming the radical cation moiety [35]. The spectrum of V_2O_5 (Figure 7b) distinct peaks at 142 cm^{-1}, 283 cm^{-1}, and 527 cm^{-1}, attributed to V-O-V lattice bending vibrations, while the strong bands at 699 cm^{-1} and 997 cm^{-1} correspond to the V-O symmetric stretching and V=O stretching modes, respectively [36, 37]. In the PANI-CSA/V_2O_5 (Figure 7c) composite, the Raman spectra retained only the red-shift of the characteristic peaks of PANI-CSA with no appearance of new Raman peaks, as shown in Figure 7. All major peaks correspond to the benzenoid and quinoid ring vibrations of PANI-CSA, indicating that the fundamental polymer backbone structure of PANI-CSA was preserved after the addition of V_2O_5.

Importantly, no new peaks emerged after the incorporation of V_2O_5, indicating that the chemical structure of PANI remained stable and that the interaction between PANI-CSA and V_2O_5 occurred primarily through physical and interfacial bonding, rather than chemical alteration of the polymer backbone. These spectral modifications corroborate the results obtained from FTIR and XRD analyses, confirming strong interfacial interactions.

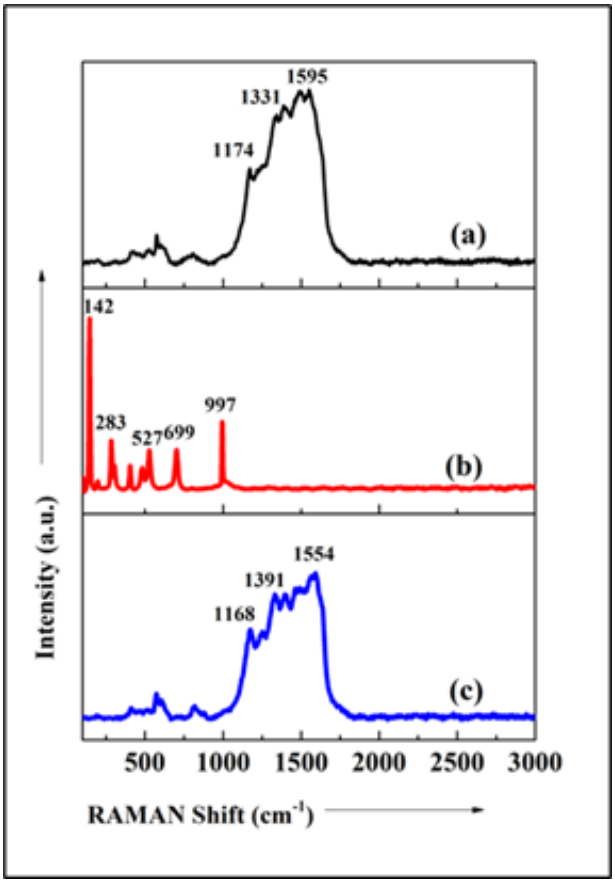

Figure 7 RAMAN spectroscopy of (a) PANI-CSA, (b) V_2O_5 and (c) PANI-CSA/V_2O_5 composite.

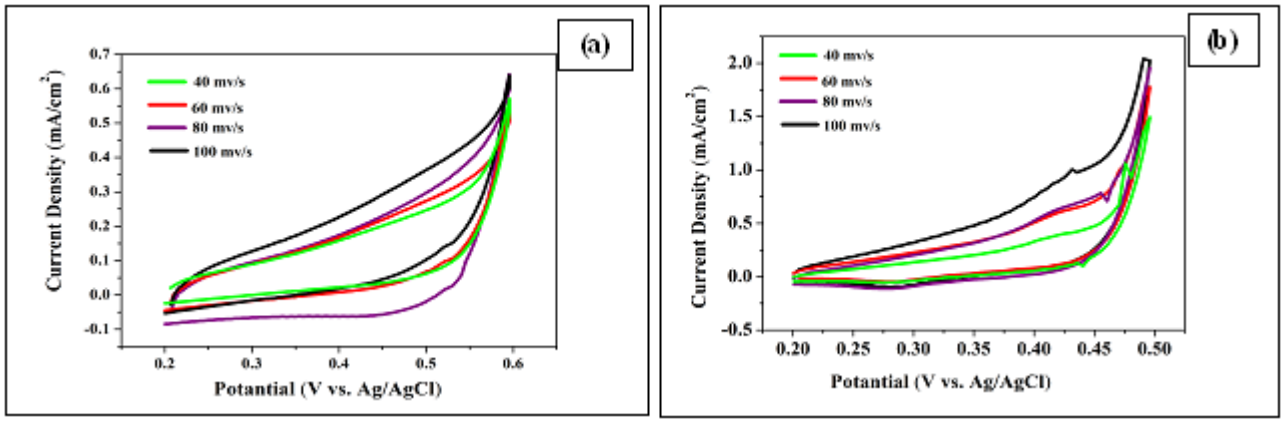

Figure 8 Cyclic Voltammetry curve of (a) PANI-CSA, (b) CV of PANI-CSA/V_2O_5 composite at different scan

The materials were electrochemically analyzed using an Ai Admiral Instruments Potentiostat, and Figures 8 (a) and (b) show the Cyclic Voltammetry (CV) curves of PANI-CSA and PANI-CSA/V_2O_5 composites, respectively. A three-electrode setup with Ag/AgCl as the reference electrode, Pt. as the counter electrode, and the synthesized material coated on a stainless-steel substrate as the working electrode was conducted in a 1 M KOH aqueous electrolyte and recorded at scan rates of 100, 80, 60, and 40 mv/s from a potential window 0.2 of 0.6v. In (Figure 8a) CV of PANI-CSA, two sets of redox peaks were observed are the characteristics of typical PANI, the first redox peak appeared between 0.2 and 0.25 v corresponding to the conversion of a fully reduced leucoemeraldine base state to the partially oxidized emeraldine state, this results additional π-electrons in the conjugate backbone and improve electrical conductivity of PANI-CSA [38,39]. Second redox peak observed between 0.55 to 0.4 v to the conversion of emeraldine to the fully oxidized form of pernigraniline [40]. However, in (Figure 8b,) CV of the PANI-CSA/V_2O_5 composite has a higher redox current and large integral area because of the large interaction of PANI-CSA with V_2O_5, which benefits the available of a more layered structure and transport to charge carriers [41]. The incorporation of V_2O_5 in PANI-CSA exhibits a higher current response of approximately 2 mA, as observed in the CV curves, indicating enhanced charge storage capability and consequently a higher specific capacitance of PANI-CSA/V_2O_5 than PANI-CSA [42].

9. Conclusion

The successful synthesis of the PANI-CSA and PANI-CSA/V_2O_5 composites through in situ polymerization using CSA was confirmed by a series of characterization techniques. UV-visible analysis revealed that the incorporation of V_2O_5 into PANI-CSA resulted in strong interaction and effective charge transfer between the polymer matrix and metal oxide. FTIR spectra confirmed the formation of hydrogen bonds and chemical interactions between the -NH groups of PANI-CSA and the oxygen atoms of V_2O_5. The XRD patterns demonstrated that the PANI-CSA/V_2O_5 composite had peaks of V_2O_5, revealing the partial crystallinity and successful intercalation of V_2O_5 into the PANI-CSA matrix. Surface morphological studies using FE-SEM and HR-TEM further supported these findings, as the spherical-granular morphology of PANI-CSA transformed into a more compact, aggregated composite structure and improved interfacial connection after the addition of V_2O_5. Raman spectroscopy confirmed the structural stability of PANI-CSA upon V_2O_5 addition, as the characteristic bands corresponding to the benzenoid and quinoid rings were retained with slight shifts and broadening, without the appearance of new peaks. This confirms the strong interaction without degradation of the PANI-CSA backbone. Generally, the combined results indicate the successful formation of a stable PANI-CSA/V_2O_5 composite with good interfacial interaction, partial crystallinity, and uniform morphology as compared to the strongly acid-synthesized PANI. The CV results showed a marked increase in current response from 0.6 mA to 2.0 mA after adding V_2O_5 in PANI-CSA, indicating improved redox activity and electrochemical conductivity of the composite. The CIF structural analysis confirms that Polyaniline exhibits a predominantly amorphous atomic arrangement with slight lattice distortions, which is consistent with the broad features observed in the XRD pattern and supports efficient charge transport along the polymer backbone.

Overall, the results demonstrate that the V_2O_5 incorporation effectively enhances the structural, morphological, and electrochemical properties of PANI-CSA, rendering the composite a promising candidate for applications in energy storage and electrochemical devices, with improved stability and performance compared to strongly acid-synthesized PANI.

Conflicts of interest: Statement No potential conflict of interest was reported by the authors

Correspondence and requests for materials should be addressed to **Jayashree A. Bagawade**

Peer review information : IRJSE thanks the anonymous reviewers for their contribution to the peer review of this work. A peer review file is available.
Reprints and permissions information is available at https://www.irjse.in/reprints

References

1. Yeszhan Y, Duisenbekov S, Kurmangaliyeva D, Kazhigitova D, Askar P, Tileuberdi Y, Konarov A, Adilov S, Nuraje N. Enhanced electrochemical performance of a polyaniline-based supercapacitor by a bicontinuous microemulsion nanoreactor approach. *RSC Advances*, 2024; 15:1205–1211. DOI: https://doi.org/10.1039/d4ra07348g.
2. Sreekala P, Honey J, Aanandan C. Development and characterization of camphor sulphonic acid doped polyaniline film with broad band negative dielectric constant for microwave applications. *Materials Research Express*, 2018; 5. DOI: https://doi.org/10.1088/2053-1591/aabe0f.
3. Jagtap S, Handore K, Adhav P, Deshpande P, Bhopale A, Khaladkar M, Khandagale P, Chabukswar V. Room temperature operating, fast and reusable polyaniline sensor synthesized ultrasonically using organic and inorganic acid dopants. *Journal of Macromolecular Science Part B*, 2022; 61:942–957. DOI: https://doi.org/10.1080/00222348.2022.2122236.
4. MacDiarmid AG. Synthetic metals: A novel role for organic polymers. *Angewandte Chemie International Edition*, 2001; 40:2581–2590. DOI: https://doi.org/10.1002/1521-3773(20010716)40:14<2581::AID-ANIE2581>3.0.CO;2-2.
5. Stejskal J, Gilbert RG. Polyaniline: Preparation of a conducting polymer. *Pure and Applied Chemistry*, 2002; 74:857–867. DOI: https://doi.org/10.1351/pac200274050857.
6. Huang J, Kaner RB. A general chemical route to polyaniline nanofibers. *Journal of the American Chemical Society*, 2004; 126:851–855. DOI: https://doi.org/10.1021/ja0371754.
7. Stejskal J, Sapurina I, Trchová M. Polyaniline nanostructures and the role of aniline oligomers in their formation. *Progress in Polymer Science*, 2010; 35:1420–1481. DOI: https://doi.org/10.1016/j.progpolymsci.2010.07.006.
8. Masemola CM, Moloto N, Tetana Z, Linganiso LZ, Motaung TE, Linganiso-Dziike EC. Advances in polyaniline-based composites for room-temperature chemiresistor gas sensors. *Processes*, 2025; 13:2–46. DOI: https://doi.org/10.3390/pr13020401.
9. Sathiyanarayanan S, Azim SS, Venkatachari G. Preparation of polyaniline–TiO_2 composite and its comparative corrosion protection performance with polyaniline. *Synthetic Metals*, 2007; 157:205–213. DOI: https://doi.org/10.1016/j.synthmet.2007.01.012.
10. Sapurina IY, Shishov MA. Oxidative polymerization of aniline: Molecular synthesis of polyaniline and the formation of supramolecular structures. *New Polymers for Special Applications*, 2012. DOI: https://doi.org/10.5772/48758.
11. Hu P, Vu TD, Li M, Wang S, Ke Y, Zeng X, Mai L, Long Y. Vanadium oxides: Phase diagrams, structural properties, and applications. *Chemical Society Reviews*, 2017; 46:6345–6378. DOI: https://doi.org/10.1021/acs.chemrev.2c00546.
12. Szymanski NJ, Liu ZT, Podraza TA, Sarin NJ, Khare SV. Electronic and optical properties of vanadium oxides from first principles. *Computational Materials Science*, 2018; 146:310–318. DOI: https://doi.org/10.1016/j.commatsci.2018.01.048.
13. Thakur YS, Acharya AD, Sharma S, Bisoyi S, Bhawna. Enhanced electrochemical performance of in situ polymerized V_2O_5–PANI nanocomposites and its practical application confirmation. *Results in Chemistry*, 2024; 7:1–15. DOI: https://doi.org/10.1016/j.rechem.2023.101259.
14. Verma A, Kumar T. Gas sensing properties of a Cu-doped PANI nanocomposite towards ammonia. *Materials Advances*, 2024; 5:7387–7400. DOI: https://doi.org/10.1039/D4MA00632A.
15. Thakur YS, Acharya AD, Sharma S, Bhawna. Enhanced electrochemical performance of PANI/V_2O_5 nanocomposites. *Journal of Materials Science: Materials in Electronics*, 2018; 29:17763–17772.
16. Bednarczyk K, Matysiak W, Tański T, Janeczek H, Balcerzak S, Libera EM. Effect of polyaniline content and protonating dopants on electroconductive composites. *Scientific Reports*, 2021; 11:74–87. DOI: https://doi.org/10.1038/s41598-021-86950-4.
17. Lenin R, Singh A, Bera C. Effect of dopants and morphology on the electrical properties of polyaniline for various applications. *Journal of Materials Science: Materials in Electronics*, 2021; 32:24710–24725. DOI: https://doi.org/10.1007/s10854-021-06883-6.
18. Shimizu K, Chinzei I, Nishiyama H, Kakimoto S, Sugaya S, Matsutani W, Satsuma A. Doped vanadium oxides as sensing materials for high temperature operative selective ammonia gas sensors. *Sensors and Actuators B: Chemical*, 2009; 141:410–416. DOI: https://doi.org/10.1016/j.snb.2009.06.048.
19. Qiu M, Zhang Y, Wen B. Facile synthesis of polyaniline nanostructures with effective electromagnetic interference shielding performance. *Journal of Materials Science: Materials in Electronics*, 2018; 29:437–444. DOI: https://doi.org/10.1007/s10854-018-9100-6.
20. Sridhar C, Yernale N. Synthesis, spectral characterization and antibacterial and antifungal studies of PANI/V_2O_5 nanocomposites. *International Journal of Chemical Engineering*, 2016; 8:1–6. DOI: https://doi.org/10.1155/2016/3479248.

21. Rahman S et al. Morphology-controlled polyaniline nanofibers via rapid polymerization for enhanced supercapacitor performance. *Nanoenergy Advances*, 2025; 15:5–11. DOI: https://doi.org/10.3390/nanoenergyadv5030011.
22. Almasi MJ, Sheikholeslami TF, Naghdi MR. Band gap study of polyaniline and polyaniline/MWNT nanocomposites. *Composites Part B*, 2016; 26:63–68. DOI: https://doi.org/10.1016/j.compositesb.2016.04.032.
23. Kwon O, McKee ML. Calculations of band gaps in polyaniline from theoretical studies of oligomers. *Journal of Physical Chemistry B*, 2000; 104:1686–1694. DOI: https://doi.org/10.1021/jp9910946.
24. Djedid N et al. Box–Behnken optimization, morphological, optical, and electrical properties of polyaniline thin films deposited using chemical bath deposition. *Journal of Macromolecular Science Part B*, 2026; 62:1–25. DOI: https://doi.org/10.1080/00222348.2026.2622503.
25. Awata R et al. High performance supercapacitor based on camphor sulfonic acid doped polyaniline/multiwall carbon nanotubes nanocomposite. *Electrochimica Acta*, 2020; 347. DOI: https://doi.org/10.1016/j.electacta.2020.136229.
26. Albaris H, Karuppasamy G. Fabrication of room temperature LPG sensor based on PANI–CNT–V_2O_5 hybrid nanocomposite. *Applied Nanoscience*, 2019; 9:1719–1729. DOI: https://doi.org/10.1007/s13204-019-00967-w.
27. Kwiatkowska E et al. Investigation of polyaniline doped with camphor sulfonic acid in chloroform solution as a hole transporting layer. *Electrochimica Acta*, 2021; 380:138264. DOI: https://doi.org/10.1016/j.electacta.2021.138264.
28. Singh M et al. Thermoelectric performance of camphor-10-sulfonic acid doped polyaniline/graphitic carbon nitride composite films. *European Physical Journal Plus*, 2022; 137:1251. DOI: https://doi.org/10.1140/epjp/s13360-022-03451-7.
29. Kaya M et al. Thickness dependent physical properties of sputtered V_2O_5 films. *Applied Physics A*, 2020; 126:830. DOI: https://doi.org/10.1007/s00339-020-04023-1.
30. Ambalagi SM et al. Dielectric properties of PANI/CuO nanocomposites. *Materials Science and Engineering*, 2018; 310:012081. DOI: https://doi.org/10.1088/1757-899X/310/1/012081.
31. Thakur YS et al. Enhanced electrochemical performance of in situ polymerized V_2O_5–PANI nanocomposites. *Results in Chemistry*, 2024; 7:101259. DOI: https://doi.org/10.1016/j.rechem.2023.101259.
32. Fuseini M, Zaghloul M, El-Shazly AH. Evaluation of synthesized polyaniline nanofibres as corrosion protection film coating. *Journal of Materials Science*, 2022; 57:6085–6101. DOI: https://doi.org/10.1007/s10853-022-06994-3.
33. Kumar N et al. Impact of Zn^{2+} doping on structural and photodiode properties of V_2O_5 nanorods. *Journal of Inorganic and Organometallic Polymers and Materials*, 2020; 31:1066–1078. DOI: https://doi.org/10.1007/s10904-020-01751-y.
34. Garrudo F et al. Pseudo-doping effect on structural and electrical properties of polyaniline. *Synthetic Metals*, 2024; 301:117523. DOI: https://doi.org/10.1016/j.synthmet.2023.117523.
35. Trchová M et al. Raman spectroscopy of polyaniline thin films. *Electrochimica Acta*, 2014; 122:28–38. DOI: https://doi.org/10.1016/j.electacta.2013.10.133.
36. Jayachandran M et al. Electrochemical performance of V_2O_5 nanostructures. *Journal of Materials Science: Materials in Electronics*, 2021; 32. DOI: https://doi.org/10.1007/s10854-021-05378-8.
37. Vekhande HN, Bagawade JA. Synthesis of graphene oxide using modified Hummers method. *Fullerenes Nanotubes and Carbon Nanostructures*, 2026; 34:251–257. DOI: https://doi.org/10.1080/1536383X.2025.2530136.
38. Bolagam R, Boddula R, Srinivasan P. Preparation of sulfonated carbon and hybrid material with polyaniline. *Journal of Solid State Electrochemistry*, 2016; 20. DOI: https://doi.org/10.1007/s10008-016-3487-x.
39. Prakash S et al. Covalently bonded polyaniline–rGO macromolecules for supercapacitors. *Journal of Power Sources*, 2026; 665:239079. DOI: https://doi.org/10.1016/j.jpowsour.2025.239079.
40. Shanmugasundaram E et al. Binder-free PANI-CQD-Cu electrode. *Nanoscale Advances*, 2024; 6:1765–1780. DOI: https://doi.org/10.1039/d3na00986f.
41. Viswanathan A, Shetty AN. High energy supercapacitor of polyaniline/vanadium pentoxide nanocomposite. *Next Sustainability*, 2025; 5:100088. DOI: https://doi.org/10.1016/j.nxsust.2024.100088.
42. Chen X et al. Synergistic effect of K^+ and PANI in vanadium oxide. *SusMat*, 2023; 3:263–275. DOI: https://doi.org/10.1002/sus2.124

Publisher's Note

IJLSCI remains neutral with regard to jurisdictional claims in published maps and institutional affiliations.